Direct Time-Resolved Observations of Vibrational Energy Flow in Weakly Bound Complexes

MICHAEL P. CASASSA

Molecular Spectroscopy Division, National Bureau of Standards, Gaithersburg, Maryland 20899

Received November 2, 1987 (Revised Manuscript Received February 16, 1988)

Contents

Michael Casassa was born in Pittsburgh, Pennsylvania. He received a B.S. degree in chemistry from the University of Pittsburgh and a Ph.D. in chemistry from the California Institute of Technology, where he worked under Kenneth Janda. He was awarded an NRC postdoctoral fellowship at the National Bureau of Standards, and is currently a permanent member of the scientific staff at NBS.

I. Introduction

Investigations of structure and vibrational dynamics in weakly bound molecular clusters[1–11] have been extraordinarily fruitful during the past 12 years, in large part due to the development of laser and molecular beam technologies.[12,13] Several excellent reviews focusing on vibrational dynamics have appeared,[6–11] and the reader is urged to refer to those for an appreciation of the scope of this field. The present article discusses direct experimental observations of the time evolution of vibrational motion leading to dissociation of isolated bimolecular and atom–molecule complexes.

In the experiments described here, complexes bound by weak intermolecular forces, e.g. van der Waals forces, hydrogen bonds, or weak covalent bonds, are vibrationally excited by laser pulses. The ensuing vibrational energy transfer processes are intramolecular vibrational relaxation (IVR) and vibrational predissociation (VP). IVR processes are those that transform an initial vibrational motion—generally an optically excited mode of a molecule in the complex—into vibrational motion in other molecular and weak-bond vibrational modes. IVR processes that lead to statistical vibrational energy distributions underlie the success of RRKM theory in describing unimolecular decomposition of isolated molecules. VP processes are fundamentally the same as IVR processes, except that they involve dissociative vibrational energy transfer into rotations and translations of the binding partners. VP can occur if the vibrational excitation exceeds the weak binding energy. The promise of direct time-resolved observations of these processes is an understanding of rates and pathways for vibrational energy flow.

Time-integrated studies[6–11] are prerequisite for performing and interpreting time-resolved experiments. Microwave, infrared, and laser-induced fluorescence (LIF) spectroscopy supply geometries and vibrational level structures of complexes. Frequency shifts of molecular vibrations upon complexation provide additional information about the intermolecular interactions. In a number of cases the line widths of individual rovibrational transitions have been measured and attributed to energy-transfer processes, the line width being proportional to the rate of decay of the spectroscopically prepared state. In other cases, rates have been inferred by deconvoluting line widths from vibrational band contours. Assignments of the rate to a VP process requires an accounting of all other relaxation channels. In simple clusters with well-resolved rotational lines such an accounting is possible,[6,14,15] and for those systems time-resolved measurements should be unnecessary. However, a comparison of a line width determination and time-resolved results has been made for only one system[16] (see section III), and there have been no comparisons for systems with individually resolved vibrational levels. For systems without resolvable rotational structure, and for more complicated

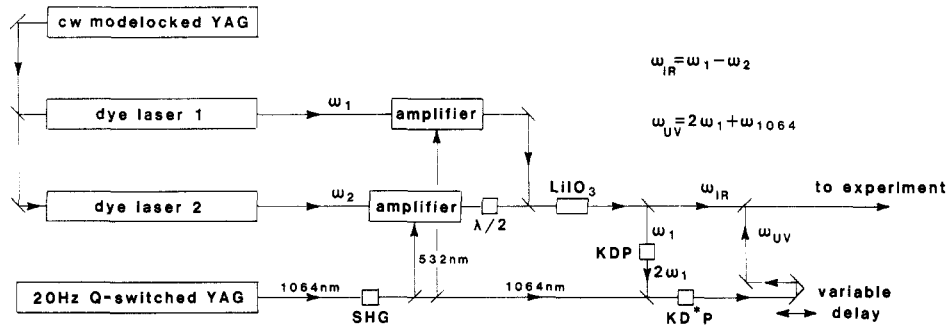

Figure 1. The picosecond laser system used for generating synchronous IR and UV pulses.

systems that have several possible line broadening processes, time-resolved measurements are essential to distinguish between and determine rates for IVR and VP.

Time-integrated studies[6-11] also can determine the intermediate and final states participating the IVR and VP processes. These are extremely sensitive probes of the interaction potential[17] and provide substantial insight into the decay mechanism. Vibrational energy flow rates may be inferred from branching ratios if the molecules in the complex provide an independent competing photophysical process of known rate by which to clock events.[18] Rates inferred in this way depend on an assumption of whether the vibrational energy flow processes occur in parallel or sequential fashion. However, with this background of information indicating which states to pump or probe, a time-resolved study can determine the rates and the sequences of participating states for vibrational energy flow processes.

Section II describes the picosecond infrared photodissociation of the NO dimer. This section includes some experimental detail and an outline of mechanistic ideas upon which subsequent discussions of IVR and VP are based. Section III describes picosecond experiments that involve electronic and vibrational excitation of large polyatomic complexes. These complexes have rich vibrational level structures, compared to the NO dimer, which provide many possible channels for vibrational energy flow. Included in section III.A is discussion of vibrational dynamics in ground electronic state Ar–*s*-tetrazine (S_0) which makes an intriguing comparison with vibronically excited Ar–*s*-tetrazine (S_1). Yet not all vibrational energy flow occurs on a picosecond time scale. Several systems with directly measured lifetimes exhibit predissociation on a much slower time scale, as discussed in section IV. Section V describes an experiment performed on CO_2–HI clusters that provides an unusual perspective for bimolecular reactions. The rate measured in that experiment is near the lower limit of time resolution for picosecond techniques. Further experiments of this type will benefit from femtosecond laser pulses.[19] A summary and concluding remarks appear in section VI. Because the scope of the discussion is restricted to time-resolved experiments, the reference list is only complete with respect to the time-resolved studies. Important theoretical and time-integrated experimental investigations are not fully cited. For the latter investigations, I have cited recent representative articles and review articles to which the reader may refer for more information.

TABLE I. Fundamental Bands of $(NO)_2$[a]

mode	symmetry	ω_0/cm^{-1}	vibrational motion
ν_1	a_1	1869[b]	symmetric NO stretch
ν_2	a_1	263	symmetric NO rocking
ν_3	a_1	170	NN stretching
ν_4	b_2	1789	antisymmetric NO stretch
ν_5	b_2	198	antisymmetric NO rocking
ν_6	a_2	88.2	torsion

[a] Reference 24. [b] Reference 30.

II. Picosecond Infrared Photodissociation: The NO Dimer

The nitric oxide dimer is an attractive system for time-resolved experiments because it has strong infrared active fundamentals and dissociation produces NO fragments that are readily detected by LIF. Much information about the ground-state structure and bonding has been obtained in spectroscopic studies of $(NO)_2$. The equilibrium geometry of the gas-phase dimer, determined by microwave spectroscopy,[20,21] is a trapezoidal structure with C_{2v} symmetry. The N–N bond distance is 2.236 Å, the ONN angle is 99.6°, and the NO bond length is 1.161 Å (0.01 Å longer than the monomer bond length). Quadrupole coupling constants determined from the microwave spectrum indicate that the unpaired π electrons of the NO partners lie in the dimer plane forming a weak N–N bond of σ symmetry. Electronic structure calculations show that a weak interaction between the oxygen atoms is responsible for the cis configuration.[22] The dimer vibrational fundamental bands and several overtone and combination bands have been observed by infrared and Raman spectroscopy.[23-25] The frequencies and assignments of the fundamental transitions are listed in Table I. The NO dimer weak bond energy determined by energy balance in infrared photodissociation experiments is $D_0 = 800 \pm 150$ cm^{-1}.[26,27] Since excitation of either of the two N–O stretching fundamentals, ν_1 or ν_4, deposits vibrational energy in the cluster that exceeds the bond energy, ν_1 and ν_4 excited clusters are metastable and eventually decay to produce NO fragments. The measured NO product state distributions[26-30] are remarkably similar for vibrational excitation of either ν_1 or ν_4. The NO fragments carry away 75–80% of the excess energy in the form of relative translational energy and the balance appears in excited rotational and spin–orbit levels. Dissociation channels involving fragment vibrational excitation are energetically inaccessible.

In order to measure the infrared photodissociation of $(NO)_2$ in real time,[29-31] picosecond infrared pulses were generated to excite ν_1 and ν_4. The NO fragments

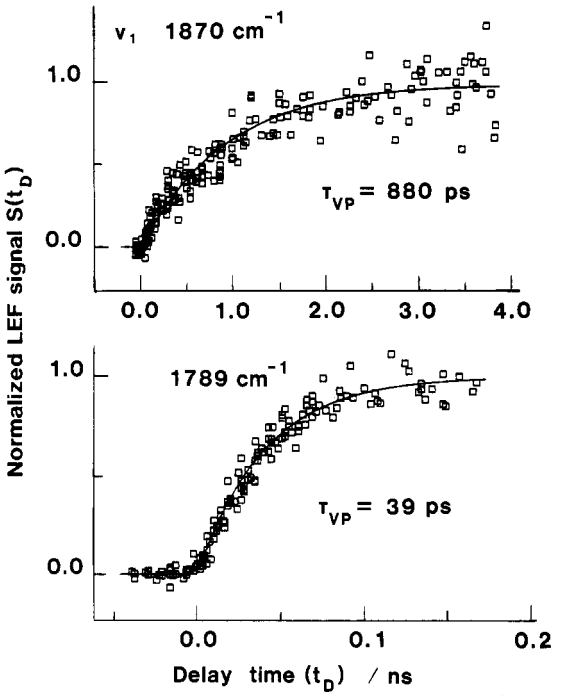

Figure 2. Time-resolved appearance of NO fragments in the X $^2\Pi_{3/2}$ state following excitation of the ν_1 and ν_4 fundamentals of $(NO)_2$. The solid curves are least-squares fits of eq 1.

were detected by LIF using ultraviolet (226 nm) picosecond pulses, delayed in time with respect to the IR excitation pulses. Figure 1 shows the laser apparatus. The pump and probe pulses were derived ultimately from a pair of dye lasers that were synchronously pumped by a mode-locked cw Nd:YAG laser. These lasers produced low-energy pulses (≈0.5 nJ) at 82 MHz having convenient wavelength tunability and short time durations (≈5 ps). Amplification using a Q-switched 2 ns Nd:YAG laser and pulsed dye amplifiers produced high-energy picosecond pulses (≈0.5 mJ) at 20 Hz. Nonlinear crystals converted the amplified visible pulses into IR pump and UV probe pulses. The dye laser wavelengths were tuned so that the difference frequency generated by mixing in a $LiIO_3$ crystal was resonant with ν_1 or ν_4. These IR pulses were directed into a molecular beam, produced by pulsed supersonic expansion of NO/He or NO/H_2 mixtures, to excite nitric oxide dimers. The 226-nm pulses necessary to excite fluorescence in the NO (A–X) system were generated from one of the visible picosecond frequencies. After the IR generation step, ω_1 was frequency doubled in a KDP crystal and further shifted to 226 nm by mixing with the fundamental of the Q-switched laser in a KD*P crystal. The arrival of the probe pulse in the molecular beam was delayed with respect to the arrival of the infrared excitation pulse by using a variable optical delay (a movable mirror). Measuring the NO fragment fluorescence intensity as a function of time delay τ_D between pump and probe pulses determined the vibrational predissociation lifetime τ_{VP}.

Data showing the time evolution of NO fragments formed following excitation of the ν_1 and ν_4 fundamentals are shown in Figure 2. These data were obtained by probing the NO $X^2\Pi_{3/2}$ spin–orbit state. Note the difference in time axes for the two data sets. It is clear that the two vibrational modes lead to dissociation with dramatically different rates. The LIF signals were fit to a simple exponential function with a unimolecular decay rate $k_{uni} = 1/\tau_{VP}$:

$$S(\tau_D) = S(\infty)[1 - \exp(-\tau_D/\tau_{VP})] \quad (1)$$

Predissociation from the lower energy, antisymmetric ν_4 mode proceeds with $\tau_{VP} = 39 \pm 8$ ps, while the higher energy ν_1 symmetric mode has a much longer lifetime, $\tau_{VP} = 880 \pm 260$ ps. The measured lifetimes are independent of the NO spin–orbit state.

The dissociation mechanism for the NO dimer is not understood, even though the dissociation rates and the fragment energy distributions have been measured. The fact that the lower energy mode dissociates at a greater rate than the higher energy mode is unexpected in terms of purely statistical theories. Instead, the difference in decay rates reflects a mode-specific coupling in the vibrationally excited complex. There are several possible coupling mechanisms, none of which can be excluded without further experimental or theoretical work.

One possibility is a direct nonadiabatic transition from the initially excited vibrational state to a repulsive electronic surface. This curve-crossing mechanism has been suggested for the related process of vibrational relaxation of NO ($v = 1$) in collisions with NO ($v = 0$), which has a large cross section compared to vibrational relaxation of O_2 and N_2.[32] For the collisional process, Nikitin[32] derived a model that shows an exponential dependence on the energy gap for the rate of transitions between two repulsive surfaces in an NO ($v = 1$) – NO ($v = 0$) collision complex. In the vibrational predissociation experiment, the energy gap would be measured from the point of crossing of the ground electronic surface (with one quantum in an NO stretching mode) and a repulsive surface. A difference in the nonadiabatic energy gaps for ν_1 and ν_4 could cause the observed mode specific lifetimes. Crossing to a repulsive surface could accelerate the fragments, giving the observed speed distributions, with a minimal degree of rotational excitation.

The efficacy of the curve-crossing mechanism depends on the energies and total symmetries (electronic plus nuclear) of the initial and final states. Nikitin suggested that the rate would be dominated by the electronic symmetries and the energy gap. Constraints on overall symmetry in the process, including the initial vibrational symmetry, could be satisfied with combinations of fragment states with appropriate overall symmetry. In the C_{2v} NO dimer, there are eight electronic states that correlate to the $^2\Pi$ electronic configurations of the separated NO partners. The ground-state $(NO)_2$ surface, upon which the vibrational motion is excited, is a $^1A_1$ state. There is experimental evidence for the existence of low-lying excited-state surfaces,[21,33] but it is inconclusive. An ab initio calculation[33] indicates that the first excited surface is a $^3B_2$ state with a vertical energy of 3630 cm^{-1} above the vibrationless ground state. This surface offers a channel for crossing from the $^1A_1$ surface since, considering only the C_{2v} electronic symmetries, the $^3B_2$ state can couple with $^1A_1$ by the spin–orbit interaction. Thus the nonadiabatic mechanism is plausible, but current knowledge provides an insufficient basis for concluding that this mechanism is actually operative. More information concerning the energies, symmetries, and couplings of the excited

electronic surfaces is needed.

The alternatives to the electronically nonadiabatic mechanism are predissociation processes mediated by vibrational potential coupling, occuring entirely on the $^1A_1$ surface. This type of coupling has been used to describe VP in many closed-shell systems.[9,10,34,35] The general ideas associated with this mechanism are mentioned here because they will recur in much of the subsequent discussion. The zero-order states are taken to be eigenfunctions of a zero-order Hamiltonian with potential energy

$$V_0(q,Q) = U(Q) + u(q,Q_e) \quad (2)$$

The first term is a function of the isolated constituents' vibrational coordinates Q and is associated with the familiar vibrational motions of the covalent bonds (e.g. ν_1 and ν_4 in NO dimer). The second term is the weak bonding potential for interaction between vibrationless partners (with atoms in some averaged or unperturbed equilibrium positions Q_e) which gives rise to vibrations in the weak-bond coordinates (e.g. ν_2, ν_3, ν_5, and ν_6 in NO dimer). At energies exceeding the weak bond strength, the weak-bond motions include fragment rotation and translation states. Excitation of covalent bond vibrations produces a perturbation

$$V_1(q,Q) = u(q,Q) - u(q,Q_e) \quad (3)$$

which mediates energy flow among the zero-order states. Equation 3 describes modulation of the cluster's weak bonding forces by excited constituent vibrations. Depending on the cluster, $V_1(q,Q)$ leads to several classes of energy-transfer processes. One class is anharmonic resonance or Fermi resonance, wherein the initial bound vibration in Q couples to other bound vibrational levels of appropriate symmetry involving both covalent and weak bond motions.[35] In experiments with sufficient spectral resolution, Fermi resonance is manifested by additional bands and perturbations that reveal the true vibrational eigenstates. Time-resolved pulsed laser experiments often have insufficient spectral resolution to resolve these eigenstates. Instead, nonstationary superposition states are excited, and their subequent time evolution is, by definition, IVR. Other classes of energy transfer produced by $V_1(q,Q)$ are VP processes, wherein the initial vibrational motion couples to translational and rotational continuum levels of the weak bond potential. For a given $V_1(q,Q)$, propensity rules for VP reflect energy and momentum gap constraints.[9,10,34,35] These constraints are related to overlap of the initial and final state wavefunctions, and they result in a preference for fragmentation channels that minimize translational energy release and changes in vibrational and rotational quantum numbers.

These ideas aid in considering whether predissociation of $(NO)_2$ is mediated by vibrational potential coupling, rather than the electronically nonadiabatic mechanisms. The high degree of anisotropy of the NO–NO interaction and the relatively small moment of inertia for NO suggest that the $(NO)_2$ $v = 1$ states should be good candidates for coupling of initial vibrational energy into fragment rotation.[34] But observations at odds with expectations for this mechanism are the large difference in decay rates for excitation of ν_1 and ν_4, and the high degree of fragment translation arising from both dissociations. In fact, a vibrational predissociation model that uses pairwise atom–atom potentials to construct $V_1(q,Q)$ indicates that the difference in energy gaps for ν_1 and ν_4 is far too small to account for the factor of 23 difference in lifetimes[31] for a process that releases energy mainly to fragment translation. However, these considerations ignore the fact that the forces contributing to $V_1(q,Q)$ may be qualitatively different for the two modes. Such a difference is indicated by the experimentally measured monomer-cluster frequency shifts, which are also determined by $V_1(q,Q)$.[35] The observed frequency shifts are -7 cm^{-1} for ν_1 and -77 cm^{-1} for ν_4 (both below the 1876-cm^{-1} monomer fundamental). Thus, ν_1 excitation weakly affects the bonding interaction, compared to ν_4 excitation which produces a 77-cm^{-1} increase in the weak bond well depth. In addition, a vibrational force field calculated for the $^1A_1$ surface shows that the weak bonding geometry is strongly affected by changes in the covalent bond lengths.[22] Thus, vibrational potential coupling with mode dependent forces in $V_1(q,Q)$ could result in the observed mode dependent predissociation lifetimes.

The situation in $(NO)_2$ is in some ways similar to other clusters that can decompose only by adiabatic vibrational predissociation. Miller has pointed out that there is a clear correlation of decay rates with frequency shifts for a large family of clusters.[15] A classic example is the hydrogen fluoride dimer, HF–HF, which exhibits resolved rotational line widths attributable to VP in its infrared spectrum.[36,37] Infrared line widths indicate that the hydrogen bound H–F stretch (ν_2, frequency shift = -93 cm^{-1}) decays in 0.5 ns while the free H–F stretch (ν_1, frequency shift = -32 cm^{-1}) decays in 12 ns. The difference in coupling for the two $(HF)_2$ modes is clearly related to the nonequivalent positions of the two oscillators. The different distortions of the cluster caused by the two vibrations lead to qualitatively different modulations of the weak bond potential. A simple geometrical origin for differences in $(NO)_2$ ν_1 and ν_4 VP is not as apparent as it is for $(HF)_2$ ν_1 and ν_2, but the dependence of the interaction potential, eq 3, on the vibrational motion could be just as significant.

III. Picosecond Dynamics Involving Vibronic Excitation

Studies of vibrational energy flow in electronically excited polyatomic van der Waals complexes take advantage of Franck–Condon factors that allow optical pumping of a wide range of vibronic modes. While these are clusters of complicated molecules with vibrational and electronic properties that often are not entirely understood, the profusion of vibrational coupling possibilities makes their study important. Several LIF studies of vibronically excited polyatomic clusters[18,38–49] have determined cluster geometries, vibrational frequencies, bond energies, IVR branching ratios, and VP fragment state distributions. The IVR and VP processes are nonstatistical, with only a few states participating in the decay processes despite a large number of energetically accessible vibrational levels.

A. Tetrazine Clusters

The time evolution of Ar–*s*-tetrazine complexes excited to low-lying vibrational levels of the S_1 state has

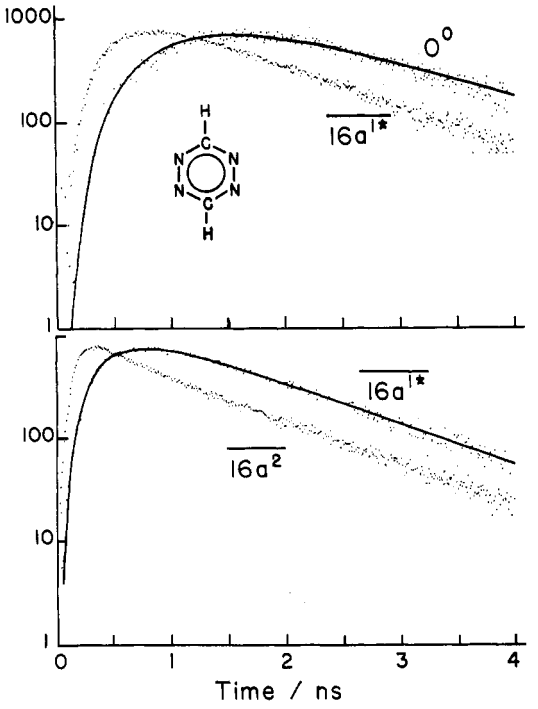

Figure 3. Time-resolved fluorescence recorded after excitation of the $\overline{16a^2}$ S_1 level of Ar–*s*-tetrazine. Emission from the initial state, an intermediate relaxed state ($\overline{16a^{1*}}$), and a fragment state (0^0) are shown. The solid curves are a fit of a sequential kinetic model (adapted from ref 50 with permission.)

been characterized in a series of experiments performed by R. P. H. Rettschnick and co-workers.[50-54] These studies provide a microscopic picture of vibrational motion evolving in parallel, competing, and consecutive rate processes leading to vibrational energy redistribution and vibrational predissociation. Rettschnick's group reported not only appearance of fragment molecules (*s*-tetrazine, S_1) and decay of the initially excited states but also observed appearance of transient intermediate states of the complexes.

The Ar–*s*-tetrazine experiments are time-resolved extensions of previous work that combined supersonic molecular beam and laser-induced fluorescence techniques in order to study the spectroscopy and photophysics of Ar–*s*-tetrazine.[18,38] The Ar–*s*-tetrazine absorption bands in the S_1–S_0 system are shifted (7–23 cm^{-1} to the red) from corresponding transitions in free *s*-tetrazine and are readily assigned. Resolved rotational structure in the LIF spectrum showed that the Ar atom resides on the out-of-plane C_2 axis with a 3.4 Å weak bond length in the S_1 state. (See the inset in Figure 3 for the tetrazine structure.) Photofragmentation observed for Ar–*s*-tetrazine (S_1) indicates that the van der Waals binding energy is $277 < D_0 < 381$ cm^{-1}. The van der Waals stretching mode has been assigned with a frequency of 43 cm^{-1}, and there is evidence that the bending mode frequencies are 17 and 19 cm^{-1}.[53]

The time-resolved studies employed a single picosecond dye laser, synchronously pumped by a mode-locked Ar^+ laser, to excite S_1 vibronic levels in jet-cooled Ar–*s*-tetrazine. The resulting fluorescence was dispersed with a monochromator. Spectral shifts allowed selective excitation of vibronic levels in the clusters as well as selective detection of levels in subsequently evolving species. Temporal profiles of selected fluorescence bands were recorded with ≈25 ps time resolution using time-correlated single photon counting.[55] Three types of emission were observed following excitation of cluster vibronic states. These were (1) unrelaxed fluorescence from the initially prepared state, (2) relaxed fluorescence emitted by intact clusters from levels other than the initially excited state, and (3) fluorescence from dissociation fragments, i.e., uncomplexed S_1 *s*-tetrazine. The second type of emission is associated with Fermi resonance mixing, as outlined in section II, and points to an IVR process in the cluster. The third type of emission indicates that a VP process occurred. Excitation of bare *s*-tetrazine produced only unrelaxed fluorescence.

Figure 3 shows time dependencies of the three types of fluorescence obtained following excitation of the $\overline{16a^2}$ level of the cluster S_1 state.[50] The bar distinguishes a vibration of the argon complex from the corresponding level in free *s*-tetrazine. Relaxed fluorescence is observed from the $\overline{16a^{1*}}$ state (where the asterisk indicates that the emitting state includes vibratonal quanta in the van der Waals modes) and fragment fluorescence was observed from the vibrationless *s*-tetrazine S_1 level, 0°. The different rise times clearly seen for the three types for emission are evidence for vibrational energy flow.

Assuming that the observed levels are the principal participants in the relaxation process, there are two possible deactivation pathways. These are either a sequential mechanism ($\overline{16a^2} \rightarrow \overline{16a^{1*}} \rightarrow 0° + Ar$) or parallel processes ($\overline{16a^2} \rightarrow \overline{16a^{1*}}$ and $\overline{16a^2} \rightarrow 0° + Ar$). The deactivation pathway can be determined by comparing observations with predictions of kinetic models, calculated by iterative convolution[51] of the time-dependent populations and the instrument response function. By this procedure, it was shown that the $\overline{16a^2}$ decay follows the sequential mechanism, and that the lifetimes (inverse rate constants) for the IVR and VP steps are 2.2 and 1.1 ns, respectively.[50] These rates are of the same magnitude as decay rates observed in isolated *s*-tetrazine excited to the same vibronic levels. The decay process that occurs in isolated *s*-tetrazine is decomposition to produce HCN and N_2. This persists in the Ar complex and competes with the vibrational predissociation. The quantum yields for IVR and VP are of the order of 10%.[18] The additional dark channel decay rates were included as fixed parameters in the kinetic modeling of the Ar–*s*-tetrazine results.

Figure 4 superimposes a partial vibrational energy level diagram for Ar–*s*-tetrazine, excluding the van der Waals bond vibrations, and a map of decay channels observed following excitation of different vibronic levels.[50] Several types of ring vibrational motion are represented, as indicated in the figure caption. Energy is conserved in the IVR process by excitation of van der Waals bond vibrations and in the VP steps by excitation of fragment rotations and translation. The rates for the elementary steps are in the range 0.2×10^9 to 3.2×10^9 s^{-1},[50] and there is no clear correlation of rates with vibrational energy. Notice that there are examples of parallel processes that feed and deplete population, as well as sequential processes. All of the observed VP processes are preceded by IVR processes. The propensity for IVR steps involving minimal changes in *s*-

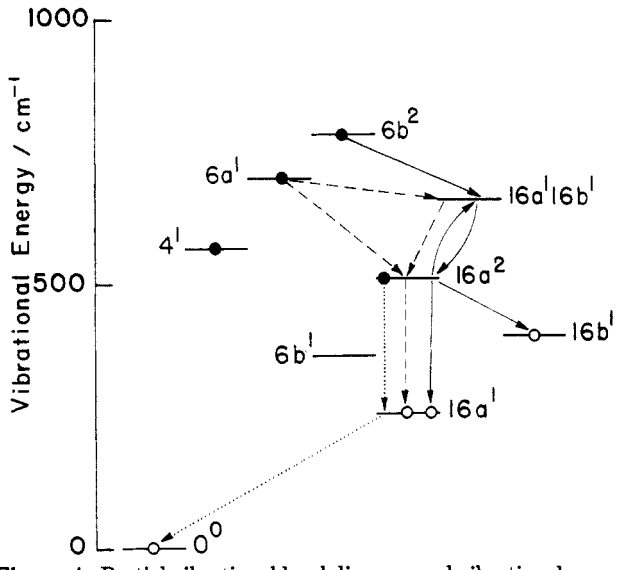

Figure 4. Partial vibrational level diagram and vibrational energy flow pathways observed for Ar–*s*-tetrazine (S_1). Paths originate with spectroscopic excitation shown as solid circles. Nondissociative IVR steps are shown as arrows. Dissociative VP steps are shown as arrows terminating at open circles. 6a and 6b are in-plane ring distortions. 4 and 16b are out-of-plane ring distortions. 16a is torsion of the ring about the C–C axis. Data shown are taken from ref 50 and 53.

tetrazine vibronic energy, as opposed to large jumps sufficient to lead to dissociation in a single step, is suggestive of an energy-gap rule similar to that mentioned for VP in section II. Sequences of steps are preferred since they tend to minimize vibrational quantum number changes.[34,35]

A detailed version of the vibrational predissociation model outlined in section II has been derived by G. E. Ewing[35] and applied to the decomposition of vibronic levels of Ar–*s*-tetrazine. This calculation shows that 16*a* Fermi resonance (i.e., mixing of the initial zeroth-order vibration with a combination of $16a^1$ and van der Waals stretching and bending modes) produces branching ratios observed in time-integrated experiments[18] for the $\overline{16a^2}$ and $\overline{6b^2}$ photodissociations. The magnitude of the calculated dissociation rates for the mixed states are in agreement with those observed in time-resolved experiments, while direct vibrational predissociations from the initial tetrazine modes are predicted to have rates as slow as 10^2 s^{-1}. The time-resolved results demonstrate that VP occurs from Fermi resonance coupled states that evolve in time from the initially excited zeroth-order state.

The $\overline{16a}$ levels play a central role in the S_1Ar–*s*-tetrazine decay sequences shown in Figure 4. The prominence of the $\overline{16a}$ IVR pathway reflects exceptionally strong coupling strengths, determined by eq 3, for the $\overline{16a}$ coordinate. Weber and Rice[56] proposed that coupling of the $\overline{16a}$ motion and vibrations of van der Waals band is particularly strong because of the symmetry of the electron charge distribution in *s*-tetrazine (S_1). They pointed out that the highest occupied electronic orbital in the S_1 state has the same nodal structure as the 16*a* normal coordinate. The $\overline{16a}$ motion is a torsion of the ring about the C–C axis. Therefore, $\overline{16a}$ motion distorts the electron cloud in such a way as to produce a repulsive interaction with the Ar atom. This idea is supported by frequency shifts of vibronic levels observed upon complexation, which indicate that the van der Waals bond is weakened upon excitation of $\overline{16a}$ levels as compared to other vibronic levels. For example, cluster $\overline{16a^2}$ bands are blue-shifted 15 cm^{-1} from the cluster S_1 origin, as compared to the monomer. Weber and Rice[56] derived a perturbation treatment that shows how this repulsive coupling underlies both the frequency shifts and $\overline{16a}$-mediated vibrational dynamics in Ar–*s*-tetrazine (S_1).

Excitation of the $\overline{4^1}$ level produced only resonant fluorescence, but the fluorescence lifetime was measurably shorter than the corresponding 4^1 lifetime.[50] While the decomposition pathway could not be determined, it may be that complexation enhances the rate of decomposition of this state of *s*-tetrazine. There are several examples (see below) of vibronic photophysics perturbed by complexation,[9] so such effects could not be completely discounted in a quantitative description of vibrational dynamics in Ar–*s*-tetrazine (S_1).

The influence of electronic structure on vibrational coupling is demonstrated by comparing results for vibrational levels in the S_1 and S_0 states of Ar–*s*-tetrazine. In order to characterize vibrational dynamics in S_0, Weber and Rice used a three-color picosecond triple resonance technique.[56] Three independently tunable wavelengths were provided by three dye lasers synchronously pumped by a mode-locked cw Nd:YAG laser. The initial state preparation used two colors, producing excited vibrational levels in S_0 by stimulated-emission pumping[57] from intermediate S_1 states. The time evolution of the S_0 vibration was monitored by LIF excited by a time-delayed pulse from the third laser. The time-resolved results showed that no significant IVR or VP occurs within a 15-ns time interval for S_0 vibrational levels in the range of 1400–2200 cm^{-1}, in stark contrast to the S_1 results. This must be a consequence of the electronic structure and its influence on the interaction potential, eq 3, since the vibrational modes, state densities, and overlap integrals are similar within the S_0 and S_1 manifolds. On the basis of the discussion above, the lack of vibrational dynamics is consistent with the observation that vibrational frequency intervals for the S_0 states exhibit small (less than 2 cm^{-1}) changes upon complexation. Similar results were obtained for S_0 levels of *s*-tetrazine bound to Kr and Xe.[56]

Emission observed following excitation of vibrations in the S_1 state of the dimethyltetrazine dimer is dominated by relaxed fluorescence.[39] This cluster bonds in a displaced-parallel-planes geometry and differs from Ar–*s*-tetrazine in that there are six instead of three vibrational modes associated with the weak bond. The dimethyltetrazine dimer also has a higher binding energy (≈1400 cm^{-1}). IVR rates for the $\overline{6a^1}$ level (517 cm^{-1}) have been determined with both line-width measurements and direct time-resolved measurements, thus providing a unique opportunity to compare results for the two methods. Homogeneous line widths determined from the fluorescence excitation spectrum indicated an IVR lifetime of 66 ± 22 ps.[39] Rice and co-workers[16] observed the evolution of the relaxed cluster emission using a time-correlated dispersed fluorescence technique to obtain an IVR lifetime of 35

± 10 ps, in agreement (within experimental uncertainty) with the line-width result.

B. Stilbene Clusters

Vibrational predissociation rates of several low-lying S_1 vibronic levels of He–*trans*-stilbene (HPhC=CPhH) have been reported by A. H. Zewail and co-workers.[58] They used picosecond time-resolved fluorescence techniques to measure the time evolution of *trans*-stilbene fragments formed in the 0^0 level (the vibrationless S_1 state) and in excited vibronic levels. The important distinction between the stilbene and *s*-tetrazine experiments is that the excited stilbene levels undergo no photochemistry, and so the observed time evolution of the stilbene complexes was attributed entirely to vibrational coupling within the S_1 state. Vibrational predissociation experiments investigated cluster levels with vibrational energy in the 0–400-cm^{-1} range, while the trans–cis isomerization of isolated *trans*-stilbene has a threshold of about 900 cm^{-1}.[59] Like Ar–*s*-tetrazine, the energy dependence of the He–*trans*-stilbene vibrational predissociation rate is nonuniform, and for a given initial state the product appearance rates differ for different products.

Exciting the $\overline{37^2}$ level at $\overline{0^0}$ + 95 cm^{-1} (two quanta in the C–Ph torsional mode[60]) led to two products, 37^1 + He and 0^0 + He, with unequal appearance rates.[58] The vibrationless product showed exponential appearance with a 45-ps time constant, while the 47-cm^{-1} 37^1 product appeared significantly faster (≤15 ps), at the limit of instrumental resolution. A kinetic scheme wherein 37^1 is formed by direct VP from $\overline{37^2}$ and 0^0 is formed by a pure IVR step followed by slower VP explains these observations. Such a scheme is consistent with Ewing's VP model[35] and with observations for Ar–*s*-tetrazine.[50] The occurrence of the 37^1 channel gives an upper limit of $D_0 < 48$ cm^{-1} fo the van der Waals bond energy.

A monotonic increase in dissociation rate as cluster vibrational energy increases is expected for statistical dissociation processes, but was not observed in He–*trans*-stilbene. Excitation of the $\overline{36^1 37^1}$ combination level at $\overline{0^0}$ + 83 cm^{-1} (one quantum of both the C–Ph out-of-plane bend and the C–Ph torsion[60]) gave only 0^0 product, with a 34-ps risetime. Excitation of $\overline{25^1}$ level at $\overline{0^0}$ + 198 cm^{-1} (the C–C–Ph in-plane bend[60]) produced stilbene fragments in an unassigned level with a risetime of 156 ps, identical with the decay time observed for resonant fluorescence from the $\overline{25^1}$ level.[58]

The results for the different initially excited modes reflect geometrical and energetic effects. The in-plane motion, $\overline{25^1}$, may couple least efficiently to the van der Waal modes since the He atom evidently bonds to stilbene above one of the phenyl groups.[46] In addition, the energy gap for a single quantum process is largest for this mode. The $\overline{37^2} \rightarrow 37^1$ channel is most efficient because it involves an out-of-plane motion, it is a one-quantum process, and it must have a small energy gap. The $\overline{37^2} \rightarrow 37^0$ process does not occur directly but proceeds via an IVR step, similar to processes directly observed in the Ar–*s*-tetrazine experiments[50] and in accord with predictions of Ewing's model.[35]

It would be of great interest to determine how intermediate states participate in the He–stilbene decomposition. It is puzzling that the $\overline{36^1 37^1} \rightarrow 36^1 37^0$ process is not observed, since the $\overline{37^2} \rightarrow 37^1$ pathway is facile. Possibly the $\overline{36^1 37^1} \rightarrow 0^0$ process observed involves an intermediate IVR step, forming for example $\overline{36^{1*}}$. Line widths determined for the $\overline{36^1 37^1}$ and $\overline{37^2}$ levels have been attributed to nondissociative IVR processes occurring in about 2 ps.[46] The time-resolved results for these states show that dissociation along certain pathways proceeds in 34 ps to 45 ps. Intermediate state detection and improved time resolution should help to discover what is happening in He–stilbene during the first few picoseconds after excitation.

At times greater than 1 ns an interesting phenomenon is observed in polarization-analyzed time-resolved fluorescence. Zewail and co-workers[61–63] demonstrated that pulsed, polarized excitation leads to fluorescence with polarization components that are modulated in time with periods given by rotational frequencies of the molecules. This is readily observed in collisionless molecular beams where only a few rotational states are populated, provided that transitions are cleanly polarized with respect to molecular axes.[63] In the case of He–*trans*-stilbene, excitation of $\overline{36^1 37^1}$ yielded product stilbene that retained the initial rotational coherence, despite the half-collision by which it was produced.[61] This shows that there is little rotational energy deposited in the fragment. In contrast, for Ne–*trans*-stilbene, the rotatonal coherence was destroyed upon fragmentation and no oscillations in the polarization-analyzed fluorescence were observed.[61] Since He is lighter than Ne, it is less able to impart rotational angular momentum to stilbene as the fragments separate.

C. Hydrogen-Bonded Aromatic Clusters

Time-resolved studies of the vibrational predissociation of several hydrogen-bonded aromatic clusters show a statistical dependence of the dissociation rates on excess vibrational energy, in contrast to the highly nonstatistical results for the rare-gas–aromatic clusters described in sections III.A and III.B. Systems of this type studied by the Zewail group include binary clusters of isoquinoline with water and methanol[64–67] and the phenol–benzene cluster.[68,69] (See the inset in Figure 5 for the isoquinoline structure.) Cluster predissociation rates were measured for a range of vibrational energies in the $^1\pi\pi^*$ state of isoquinoline and in the S_1 state of phenol.

Dissociation of the hydrogen-bonded clusters was characterized by time-resolving the disappearance of the initially excited parent clusters. This was accomplished for the isoquinoline clusters by using a time-correlated dispersed fluorescence technique. Spectral shifts of absorption and emission bands in the H_2O and CH_3OH complexes, compared to bands of isolated isoquinoline, allowed selective excitation and detection of the clusters.[64,65] The phenol clusters were studied by using a picosecond photoionization mass spectrometry technique.[68,69] The probe pulse ionized the vibronically energized clusters and the resulting cluster ions, $(C_6H_6OH–C_6H_6)^+$, were mass filtered and detected by time-of-flight mass spectrometry. Knee et al.[68] argue that if the photoionizing light is tuned sufficiently above threshold, both the initial vibronically excited level and

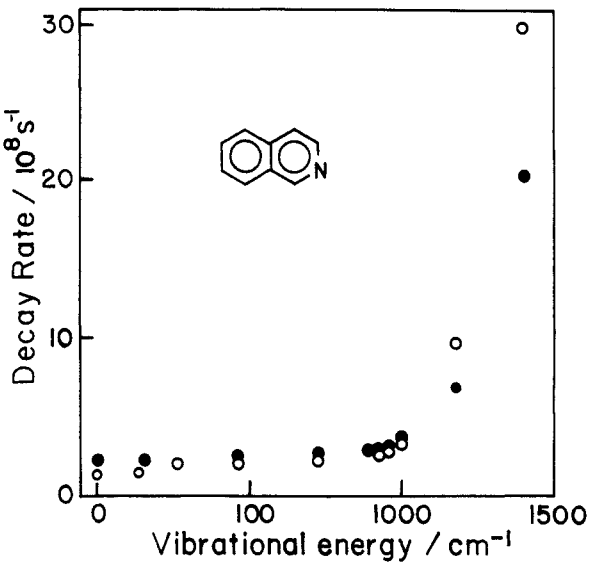

Figure 5. Decay rates as a function of vibrational energy observed for isoquinoline, drawn in the figure, bound to H_2O (open circles) and bound to CH_3OH (filled circles) (adapted from ref 67 with permission).

clusters that may have undergone vibrational energy redistribution are ionized with equal probability. Thus, the probe is sensitive only to dissociation and not intermediate IVR. Time delays were varied in the photoionization experiments by scanning optical delays. Compared to the time-resolved dispersed fluorescence technique, the photoionization method is perhaps more general and offers better time resolution, limited only by the laser pulse widths. On the other hand, the fluorescence technique permits selective detection of fragment states and initial and intermediate states of the clusters.

Figure 5 shows the measured decay rates as a function of vibrational energy for the isoquinoline clusters. These two systems and the phenol–benzene cluster exhibit energy thresholds above which rates increase monotonically with energy. The thresholds (1000 cm^{-1} for isoquinoline, 1400 cm^{-1} for phenol) are consistent with the expected 3–4 kcal/mol hydrogen bond energies. With use of reasonable values for the vibrational frequencies and for the barriers to dissociation, all three data sets can be simulated qualitatively by RRKM theory.[66-68] This suggests that IVR producing statistical vibrational energy distributions precedes cluster fragmentation, in contrast to the results for the rare-gas van der Waals clusters described in sections III.A and III.B. It seems plausible that energy randomizes in the hydrogen-bonded clusters, but not in the rare-gas clusters, because the former have more vibrational modes that provide channels for IVR. In the hydrogen-bonded clusters there are six low frequency modes associated with the weak bond, instead of three for the rare-gas clusters, and there are the additional internal modes of the initially vibrationless partner. Also, the coupling for IVR processes may be stronger in hydrogen-bonded clusters than in rare-gas van der Waals molecules.

Whether the molecular vibrations of the initially vibrationless partner (H_2O, CH_3OH, or C_6H_6) become statistically involved in the decomposition is an interesting question. Experimentally, identification of intermediate states could provide an answer. A quantitative comparison of RRKM theory and experimental dissociation rates might indicate which modes of the cluster participate in IVR and dissociation.[66,68] Unfortunately, the information about excited cluster vibrations that is required to make a meaningful comparison is not available.

Not all hydrogen-bonded aromatics give statistical results. While the phenol–benzene results could be modeled with a single first-order rate constant, *p*-methylphenol–benzene exhibits nonexponential decay that can be fit by using a biexponential decay model.[68] The rates and relative contributions of the individual components vary somewhat irregularly with energy, but the general trend shows the overall decay rates increase with excess vibrational energy. A possible explanation invokes IVR into distinct regions of phase space, from which decompositions proceed on different time scales.[68] This has some appeal since the methyl group presents an additional energy-accepting reservoir, and methyl rotors have been shown to be active in other IVR processes.[70,71] However, confirmation of this type of hypothesis clearly would require observation of the intermediate states.

The above discussion of vibrational energy flow ignores energy-transfer processes involving the electronic degrees of freedom. Vibronic mixing in isoquinoline[72-74] and phenol[75] are strongly affected by complexation.[64,65,68,74,75] It appears that the vibronic level structure is actually simplified in the clusters, at least at the relatively low vibrational energies discussed here. Both molecules undergo a nonradiative process that is quenched in the complexes. At energies where no vibrational predissociation occurs, near the S_1 origin, the resonant fluorescence from the phenol–benzene cluster (excited to $\overline{0^0}$ + 782 cm^{-1} vibrational energy) has a >5-ns lifetime (too long to be measured easily with optically delayed picosecond pulses), while the same state of the phenol monomer has a 1–2-ns lifetime.[68] The lifetimes of isoquinoline states in the CH_3OH and H_2O clusters are more than a factor of 10 longer than the corresponding states in the bare molecule.[64,65,67] In isoquinoline, interaction of the $\pi\pi^*$ state with a neighboring $n\pi^*$ state is thought to give rise to perturbations in the $\pi\pi^*$ spectrum and an enhanced rate of internal conversion.[72-74] Upon complexation with a polar molecule, the $n\pi^*$ state shifts to higher energy, bands attributed to the mixed vibronic levels disappear,[74] and the radiationless rate decreases.[64,65]

IV. Time-Resolved Measurements in the Nanosecond and Microsecond Regimes

All of the preceding experiments used picosecond laser techniques to observe energy flow and fragmentation in clusters, but picosecond technology is clearly inappropriate for many vibrational predissociation processes.[6-10,15] Calculations have shown that predissociation rates are extremely sensitive to the nature of the intermolecular interaction and the number of degrees of freedom of the constituents.[9,10,34] There is now firm experimental evidence that predissociation events happen on a wide range of time scales. Real-time measurements have resolved lifetimes as short as 34 ps [He–stilbene (S_1, $\overline{36^1 37^1}$)],[58] and metastable vibrationally excited clusters have been observed to survive for more than 0.3 ms [Ar–HF (v = 1)].[76] The following

section on rare-gas–halogen complexes recounts measurements that determined nanosecond and microsecond vibrational predissociation lifetimes. The ethylene clusters section includes two other nanosecond techniques that provide upper limits for predissociation lifetimes.[77]

A. Rare-Gas–Halogen Clusters

Vibrational predissociation of van der Waals molecules was first observed for $He–I_2$ in pioneering experiments reported by Smalley, Levy, and Wharton.[78] The triatomic rare-gas–halogen clusters have since proven to be amenable to experimental and theoretical investigations,[9-11] and they are perhaps the best characterized of the vibrationally predissociating systems.[17,79] The diatomic halogen partners have electronic transitions that are accessible to visible and UV lasers with significant Franck–Condon factors over a wide range of vibrational levels. Rotationally resolved spectra and product state distributions for vibrational predissociations have been obtained for several vibronic levels of these clusters. In many instances, predissociation lifetimes may be inferred from homogeneous line widths observed in the spectra. In these simple systems, it is generally agreed that there are no competing broadening mechanisms. However, in some cases, homogeneous line widths cannot be resolved because of limits on spectral resolution or because of spectral congestion.

A time-resolved nanosecond technique was used by M. I. Lester and co-workers to measure the following vibrational predissociation lifetimes:[80,81]

$$\text{Ne–ICl (A, } v = 14) \xrightarrow[\tau_{VP} = 3 \pm 2 \text{ ns}] \text{ ICl (A, } v = 13, \text{ J) + Ne}$$

$$\text{Ne–ICl (B, } v = 2) \xrightarrow[\tau_{VP} > 50 \text{ ns}] \text{ ICl (B, } v = 1, \text{ J) + Ne}$$

$$\text{He–ICl (B, } v = 2) \xrightarrow[\tau_{VP} < 1 \text{ ns}] \text{ ICl (B, } v = 1, \text{ J) + He}$$

The figures in parentheses indicate the ICl electronic and vibrational state. The initial states dissociate with the transfer of one quantum of diatom vibrational energy to the van der Waals bond. Two pulsed tunable dye lasers pumped by a single excimer laser were used for these measurements. One laser excited the initial level via a B ← X (or A ← X) ICl transition. Optically delayed pulses from the second laser were used for LIF detection of both the metastable clusters and the fragments via E ← B (or E ← A) ICl transitions. The ratio of the excited cluster intensity and the fragment intensity was measured as a function of time delay to determine the lifetimes. Using this ratio precludes artifacts introduced by the necessarily long optical delays in the nanosecond time regime (it can be extremely difficult to propagate a pulsed laser beam several meters without seriously altering its focal properties). The lifetime with the 1-ns upper limit represents the lower limit of time resolution for the nanosecond laser system. The lifetime with the 50-ns upper limit is determined by the maximum optical delay. Lifetimes in excess of 100 ns become difficult to measure in pump–probe experiments since the molecular beam flow (10^5 cm s^{-1}) moves the excited volume out of the field of view of the probe pulse during long time delays.

The vibrationial predissociation lifetime for $Ne–Br_2$ (X, $v = 1$) has been determined by taking advantage of the molecular beam flow velocity. K. C. Janda and colleagues[82] have observed metastable $Ne–Br_2$ (X, $v = 1$) clusters formed in supersonic expansions. Evidently the vibrational predissociation process,

$$\text{Ne–Br}_2 \text{ (X, } v = 1) \rightarrow \text{Br}_2 \text{ (X, } v = 0, \text{ J) + Ne}$$

is quite slow, leading to observation of metastable clusters several millimeters downstream from the nozzle. A method similar to that used for fragment detection in the ICl experiments was used to generate signals proportional to the metastable cluster number density. The $Ne–Br_2$ (X, $v = 1$) population was pumped to the $Ne–Br_2$ (B, $v = 10$) state, which predissociates in 355 ps (determined by a line-broadening measurement[83]) to produce Br_2 (B, $v = 9$). These intermediate fragments were then pumped to the E state, which fluoresces with intensity proportional to the initial $Ne–Br_2$ (X, $v = 1$) concentration. The fluorescence signal was measured as a function of time delay between cluster formation and detection, by varying the distance between the nozzle and the detection laser beams. The signals were normalized to the uncomplexed Br_2 (X, $v = 1$) signal to account for the concentration gradient in the expanding gas jet. This yielded a predissociation lifetime of 8 ± 3 μs. While this lifetime is significantly longer than lifetimes for $Ne–Br_2$ (B, $v = 11$ through $v = 30$) determined by linewidth measurements,[83] the (X, $v = 1$) lifetime is in reasonably good agreement with an extrapolation of an energy gap rule that fits the B state data.[82] This suggests that most of the excess energy released in the (X, $v = 1$) predissociation appears in fragment translation, as has been observed for the B state vibrational predissociations.

B. Ethylene-Containing Clusters

The vibrational dynamics and infrared spectroscopy of ethylene clusters have received considerable attention during the past decade. Interest began with the discovery that $(C_2H_4)_2$ can be photodissociated over the entire 200-cm^{-1} range of a pulsed CO_2 laser.[84] These frequencies excited the ν_7 out-of-plane hydrogen bending fundamental. The subsequent history of this mysterious transition has been discussed in articles by Gentry,[85] Miller,[7] Celii,[8] and Janda.[9] Many observations of the ν_7 photodissociation spectrum of $(C_2H_4)_2$ and other ethylene-containing clusters, obtained with CO_2 lasers and mass spectrometric detection, showed broad, structureless bands.[85] Originally the widths were attributed to VP,[86] but time has revealed a certain naiveté in this view. Gentry has proposed a model that attributes these contours to unresolved Fermi resonance-induced transitions.[85,87] Recent experiments suggested that under some conditions the $(C_2H_4)_2$ (ν_7) spectrum has components that arise from at least two distinct ensembles of dimers.[88] A sharp structured spectrum, with 3.5-MHz linewidths, is superimposed on a homogeneous 12 cm^{-1} wide background.[88] The widths correspond to 50 ns and 0.4 ps decay processes, respectively. Because of the possibility of contributions from larger C_2H_4 clusters, there has been some dis-

agreement over whether the broad spectrum can be attributed to the dimer.[89] While the observation of multiple dimer ensembles is an intriguing complication that must be further investigated, a central question remains unanswered: What is(are) the vibrational predissociation rate(s)? The time-resolved nanosecond experiments described below directly addressed this question and provided 10-ns upper limits for the dissociation lifetimes of $(C_2H_4)_2$ (ν_7) and NO–C_2H_4 (ν_7).

Gentry and co-workers observed dissociation of $(C_2H_4)_2$ (ν_7) by exciting first with a pulsed CO_2 laser and measuring disappearance of the excited dimers by time-delayed multiphoton ionization.[90] The ionization pulse was produced by a frequency-tripled Nd:YAG laser and a time-of-flight mass spectrometer was used to detect ions arising from the dimer. Measurements of the fragment signal as a function of delay time between the IR and UV pulses showed a pulse-width limited response, i.e., the predissociation lifetime is less than 10 ns. It seems that these time-resolved signals were primarily due to the species that exhibit the broad (0.4 ps) spectrum. The species responsible for the sharp (50 ns) structure may actually have a dissociation lifetime longer than the range of these time-resolved measurements (100 ns). Alternatively, the long-lived species may have been excited in insufficient numbers to significantly influence the results.

Infrared photodissociation of NO–C_2H_4 (ν_7) has been characterized by King and Stephenson using a nanosecond IR pump–UV probe techniques.[91] CO_2 laser pulses of 2-ns duration excited ν_7 in the clusters, and NO product states were determined by LIF using 9-ns duration UV pulses. Again, the results give a 10-ns upper limit for the dissociation time. The lifetime estimated from the width of the NO–C_2H_4 (ν_7) photodissociation spectrum is 0.7 ps, and so the origin of the width remains unknown.

V. Time-Resolved Studies of Bimolecular Reactions: CO_2–HI

Direct observation of the decay of the energized complex formed in a bimolecular reaction is possible with use of time-resolved techniques and bimolecular clusters of the reagents or precursors. If the reaction can be photochemically triggered, then a short laser pulse can be used to initiate reaction in a cluster and establish a time origin for time-delayed probe measurements. The cluster vibrational predissociation experiments are a special case corresponding to collisional vibrational energy transfer for a restricted range of impact parameters, geometries, and energies. But it is also possible to study bimolecular reactions that involve breaking and forming covalent bonds, as demonstrated in a time-integrated experiment performed by Wittig and co-workers.[92] They observed the fragmentation of an activated complex for the reaction H + CO_2 → OH + CO by photochemically initiating the reaction in CO_2–HBr clusters. Scherer, Khundar, Bernstein, and Zewail[93] reported time-resolved measurements of product appearance for the same reaction initiated in CO_2–HI clusters.

Scherer and colleagues[93] formed CO_2–HI in supersonic expansions and photolyzed the HI partner with 239 nm picosecond pusles. This produced H atoms with kinetic energies of 112 or 200 kJ mol^{-1} (depending on the I fragment spin–orbit state). The structure of CO_2–HI has not been measured, but the structures of CO_2–HF and CO_2–HCl are well known.[94,95] These have hydrogen-bonded linear structures, with O–H bond lengths of about 2 Å. Zero point bending motion displaces the light H atom about 25° off the intermolecular axis in the vibrationally averaged structure. Assuming this cluster geometry for CO_2–HI, the hot H atom produced by HI photolysis is propelled toward the CO_2 partner with a range of trajectories that should be favorable for reaction. The H atom kinetic energy exceeds the barrier to formation of HOCO*, and energy redistribution in nascent HOCO* leads to fragmentation to form OH + CO. The rate for the overall process was measured by detecting the OH fragment with LIF excited by time-delayed 308-nm pulses. Figure 6 shows the exponential growth of OH concentration as a function of time after the initiation pulse. Data of this type suggest that the HOCO* lifetime is 5 ± 2 ps, which is at the lower limit of time resolution for the picosecond pulses.

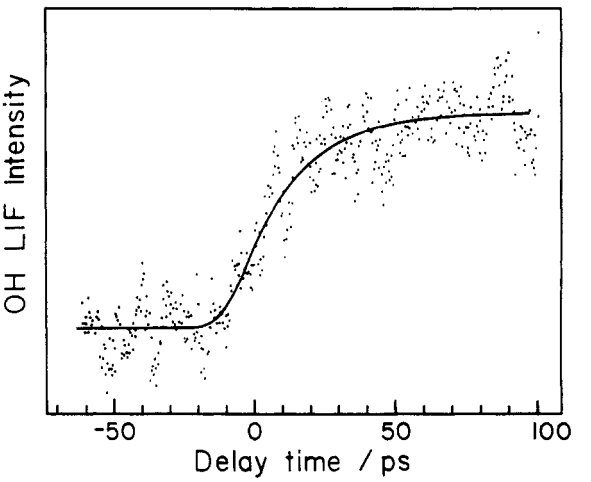

Figure 6. Time-resolved appearance of the OH fragment, measured by LIF, following photochemical initiation of the H + CO_2 reaction in the CO_2–HI complex. The solid curve is a fit of an exponential rise (eq 1) (adapted from ref 93 with permission.)

Becuse of the unusual circumstances of this bimolecular reaction, i.e., the reaction is initiated in a cluster, it is important to examine CO_2–HI even more closely. It should be feasible to probe all of the fragments with shorter time resolution. Since the I atom moves less than 2 Å during the first picosecond of reaction, it may play a role in the short time dynamics. The possibility that the halogen atom influences the course of the reaction was pointed out by Wittig and co-workers[92] in their study of product state distributions for the H + CO_2 reaction in CO_2–HBr clusters. Also, the assumption that the observed OH transient is dominated by decay of HOCO* may not be true for all H atom energies and trajectories. At higher energies, for example, the reaction may proceed in a direct fashion. Direct detection of HOCO* itself would shed some light on this problem.

VI. Summary

The time-resolved measurements described here have provided a fascinating glimpse of molecular vibrational states evolving in real time. In $(NO)_2$ a dramatic and so far unexplained mode-specific dissociation was ob-

served by measuring the appearance rate of products. The NO dimer is unique among the vibrationally excited clusters because of the presence of low-lying electronic surfaces and the possibility of a nonadiabatic transitions. Vibronic excitation of larger clusters produced mode-specific vibrational energy flow in some cases, and essentially statistical dissociation in others. In Ar–*s*-tetrazine vibrational population was observed cascading through vibrational levels in the S_1 state of the cluster, but no population flow was observed (in a 15-ns time interval) in the S_0 state. Finally, a photochemical reaction in CO_2–HI clusters was used to observe a bimolecular reactions in real time.

It is always interesting to speculate on what the future holds. For small molecules excited to low-lying vibrations to the infrared, or for the rare-gas–halogen clusters, a complete experimental description of vibrational predissociation can be realized. Excitation spectra, fragment state distributions, and lifetime measurements combined can be compared with results of accurate calculations to characterize the weak bonding potential and its dependence on constituent molecular vibrations. Alternatively, experimental results can be used to test approximate methods that would be practical to apply to complicated systems. Lifetimes based on resolved line widths are presumed to be unambiguous for the simplest systems, but as a test, real time measurements are necessary for some representative systems. In the absence of rotational resolution, and for clusters like $(C_2H_4)_2$ with complicated spectroscopy at the $v = 1$ level, the time-resolved measurements are essential.

The time-resolved results for the S_0 and S_1 states of Ar–*s*-tetrazine show that there is a great deal to be learned about vibrational energy flow from studying clusters containing large molecules with several vibrational degrees of freedom. Such experiments can provide a qualitative understanding of how intermolecular forces control the rates and pathways for vibrational energy flow. Time-resolved studies of vibrational energy flow in S_1 clusters should be expanded to include the initial, intermediate, and final states of many of the systems that have been so well characterized with the time-integrating methods. The results for S_0 Ar–tetrazine were surprising and instructive, but is is doubtful that vibrational coupling will be as weak for other ground electronic state clusters. The stimulated-emission pumping method can be used to populate highly excited vibrational levels in the ground electronic state and should prove to be a valuable tool for advancing the study of vibrational dynamics in clusters.

As the CO_2–HBr and CO_2–HI experiments suggest, photochemical reactions in clusters can be used to generate extremely energetic species, whose subsequent decay can be followed in real time. There are many other candidates for this type of study. Time-resolved experiments with femtosecond time resolution and the detection of intermediate species as well as fragments would be a spectacular accomplishment and could significantly enhance understanding of transition states and bimolecular reactions.

VII. Acknowledgment

I am pleased to thank my NBS colleagues R. R. Cavanagh, G. T. Fraser, E. J. Heilweil, D. S. King, A. S. Pine, and J. C. Stephenson for their comments on this manuscript. Thanks also to Professors K. C. Janda, M. I. Lester, R. P. H. Rettschnick, S. A. Rice, M. R. Topp, and A. H. Zewail, and Dr. P. M. Weber for suggestions, reprints, and preprints.

Registry No. $(NO)_2$, 16824-89-8; Ar, 7440-37-1; He, 7440-59-7; CO_2, 124-38-9; HI, 10034-85-2; *s*-tetrazine, 290-96-0; *trans*-stilbene, 103-30-0; ethylene, 74-85-1.

References

(1) Characterization of weak bonding and other properties of clusters have received considerable attention because of their relationship to condensed phase properties. Reference 2 is a recent review that summarizes the breadth of cluster research. References 3–5 are journal issues that, like this volume, are devoted to the study of van der Waals molecules and other clusters. References 6–11 are review articles that are more concerned with vibrational properties of clusters.
(2) Castleman, A. W., Jr.; Keesee, R. G. *Annu. Rev. Phys. Chem.* **1986**, *37*, 525.
(3) "Gas-Phase Clusters", *Chem. Rev.* **1986**, *86*, 491.
(4) *Ber. Bunsenges. Phys. Chem.* **1984**, *88*, 187.
(5) "Van der Waals Molecules", *Faraday Discuss. Chem. Soc.* **1982**, *73*, 1.
(6) Nesbitt, D. J. *Chem. Rev.*, accompanying paper in this issue.
(7) Miller, R. E. *J. Phys. Chem.* **1986**, *90*, 3301.
(8) Celii, F. G.; Janda, K. C. *Chem. Rev.* **1986**, *86*, 507.
(9) Janda, K. C. *Adv. Chem. Phys.* **1985**, *60*, 201.
(10) Beswick, J. A.; Jortner, J. *Adv. Chem. Phys.* **1981**, *47*, 363.
(11) Levy, D. H. *Adv. Chem. Phys.* **1981**, *47*, 323.
(12) Levy, D. H. *Annu. Rev. Phys. Chem.* **1980**, *31*, 197.
(13) Hayes, J. M. *Chem. Rev.* **1987**, *87*, 745.
(14) Jucks, K. W.; Miller, R. E. *J. Chem. Phys.* **1987**, *86*, 6637.
(15) Miller, R. E., to be published.
(16) Smith, D. D.; Lorincz, A.; Siemion, J.; Rice, S. A. *J. Chem. Phys.* **1984**, *81*, 2295.
(17) Halberstadt, N.; Beswick, J. A.; Janda, K. C. *J. Chem. Phys.* **1987**, 3966 and references therein.
(18) Brumbaugh, D. V.; Kenny, J. E.; Levy, D. H. *J. Chem. Phys.* **1983**, *78*, 3415.
(19) Fleming, G. R. *Annu. Rev. Phys. Chem.* **1986**, *37*, 81.
(20) Kukolich, S. G. *J. Mol. Spectrosc.* **1983**, *98*, 80.
(21) Western, C. M.; Langridge-Smith, P. R. R.; Howard, B. J.; Novick, S. E. *Mol. Phys.* **1981**, *44*, 145.
(22) Skaarup, S.; Skancke, P. N.; Boggs, J. E. *J. Am. Chem. Soc.* **1976**, *98*, 6106.
(23) Dinerman, C. E.; Ewing, G. E. *J. Chem. Phys.* **1970**, *53*, 626.
(24) Menoux, V.; LeDoucen, R.; Haeusler, C.; Deroche, J. C. *Can. J. Phys.* **1984**, *62*, 322.
(25) Brechignac, Ph.; DeBenedictus, S.; Halberstadt, N.; Whitaker, B. J.; Avrillier, S. *J. Chem. Phys.* **1985**, *83*, 2064.
(26) Casassa, M. P.; Stephenson, J. C.; King, D. S. *J. Chem. Phys.* **1986**, *85*, 2333.
(27) Casassa, M. P.; Stephenson, J. C.; King, D. S. *Faraday Discuss. Chem. Soc.* **1986**, *82*, 251.
(28) Brechignac, Ph.; Halberstadt, N.; Whitaker, B. J.; Coutant, B. *Chem. Phys. Lett.* **1987**, *142*, 125.
(29) Casassa, M. P.; Stephenson, J. C.; King, D. S. In *Structure and Dynamics of Weakly Bound Molecular Complexes*; Weber, A., Ed.; D. Reidel Publishing Co.: Dordrecht, 1987; p 513.
(30) Casassa, M. P.; Stephenson, J. C.; King, D. S. *J. Chem. Phys.*, in press.
(31) Casassa, M. P.; Woodward, A. M.; Stephenson, J. C.; King, D. S. *J. Chem. Phys.* **1986**, *85*, 6235.
(32) Nikitin, E. E. *Opt. Spectrosc.* **1960**, *9*, 8.
(33) Ha, T.-K. *Theor. Chim. Acta* **1981**, *58*, 125.
(34) Ewing, G. E. *Faraday Discuss. Chem. Soc.* **1982**, *73*, 325.
(35) Ewing, G. E. *J. Phys. Chem.* **1986**, *90*, 1790.
(36) Pine, A. S.; Lafferty, W. J. *J. Chem. Phys.* **1983**, *78*, 2145.
(37) Huang, Z. S.; Jucks, K. W.; Miller, R. E. *J. Chem. Phys.* **1986**, *85*, 3338.
(38) Haynam, C. A.; Brumbaugh, D. V.; Levy, D. H. *J. Chem. Phys.* **1984**, *80*, 2256.
(39) Haynam, C. A.; Brumbaugh, D. V.; Levy, D. H. *J. Chem. Phys.* **1984**, *81*, 2282.
(40) Butz, K. S.; Catlett, D. L., Jr.; Ewing, G. E.; Krajnovich, D.; Parmenter, C. S. *J. Phys. Chem.* **1986**, *90*, 3533.
(41) Abe, H.; Ohyanagi, Y.; Ichijo, M.; Mikami, N.; Ito, M. *J. Phys. Chem.* **1985**, *89*, 3512.
(42) Kobayashi, T.; Kajimoto, O. *J. Chem. Phys.* **1987**, *86*, 1118.
(43) Rosman, R. L.; Rice, S. A. *J. Chem. Phys.* **1987**, *86*, 3292.
(44) Halberstadt, N.; Soep, B. *J. Chem. Phys.* **1984**, *80*, 2340.
(45) Zwier, T. S.; Carrasquillo, E.; Levy, D. H. *J. Chem. Phys.* **1983**, *78*, 5493.

(46) Taatjes, C. A.; Bomsa, W. B.; Zwier, T. S. *Chem. Phys. Lett.* **1986**, *128*, 127.
(47) Mangle, E. A.; Topp, M. R. *J. Phys. Chem.* **1986**, *90*, 802.
(48) van Herpen, W. M.; Meerts, W. L.; Dymanus, A. *J. Chem. Phys.* **1987**, *87*, 182.
(49) Even, U.; Amirav, A.; Leutwyler, S.; Ondrechen, M. J.; Berkovitch-Yellin, Z.; Jortner, J. *Faraday Discuss. Chem. Soc.* **1982**, *73*, 153.
(50) Heppener, M.; Rettschnick, R. P. H. In *Structure and Dynamics of Weakly Bound Molecular Complexes*; Weber, A., Ed.; D. Reidel Publishing Co.: Dordrecht, 1987; p 553.
(51) Heppener, M.; Kunst, A. G. M.; Bebelaar, D.; Rettschnick, R. P. H. *J. Chem. Phys.* **1985**, *83*, 5341.
(52) Ramaekers, J. J. F.; Krijnen, L. B.; Lips, H. J.; Langelaar, J.; Rettschnick, R. P. H. *Laser Chem.* **1983**, *2*, 125.
(53) Ramaekers, J. J. F.; van Dijk, H. K.; Langelaar, J.; Rettschnick, R. P. H. *Faraday Discuss. Chem. Soc.* **1983**, *75*, 183.
(54) Ramaekers, J. J. F.; Langelaar, J.; Rettschnick, R. P. H. In *Picosecond Phenomena III*; Eisenthal, K. B., et al., Eds.; Springer-Verlag: West Berlin, 1982; p 264.
(55) Turko, B. T.; Nairn, J. A.; Sauer, K. *Rev. Sci. Instrum.* **1983**, *54*, 118.
(56) Weber, P. M.; Rice, S. A. *J. Chem. Phys.* **1988**, *88*, 6120.
(57) Hamilton, C. E.; Kinsey, J. L.; Field, R. W. *Annu. Rev. Phys. Chem.* **1986**, *37*, 493.
(58) Semmes, D. H.; Baskin, J. S.; Zewail, A. H. *J. Am. Chem. Soc.* **1987**, *109*, 4104.
(59) Amirav, A.; Jortner, J. *Chem. Phys. Lett.* **1983**, *95*, 295.
(60) Spangler, L. H.; van Zee, R.; Zwier, T. S. *J. Phys. Chem.* **1987**, *91*, 2782.
(61) Baskin, J. S.; Semmes, D. H.; Zewail, A. H. *J. Chem. Phys.* **1986**, *85*, 7488.
(62) Baskin, J. S.; Felker, P. M.; Zewail, A. H. *J. Chem. Phys.* **1986**, *84*, 4708.
(63) Felker, P. M.; Zewail, A. H. *J. Chem. Phys.* **1987**, *86*, 2460.
(64) Felker, P. M.; Zewail, A. H. *Chem. Phys. Lett.* **1983**, *94*, 448.
(65) Felker, P. M.; Zewail, A. H. *Chem. Phys. Lett.* **1983**, *94*, 454.
(66) Khundkar, L. R.; Marcus, R. A.; Zewail, A. H. *J. Phys. Chem.* **1983**, *87*, 2473.
(67) Felker, P. M.; Zewail, A. H. *J. Chem. Phys.* **1983**, *78*, 5266.
(68) Knee, J. L.; Khundkar, L. R.; Zewail, A. H. *J. Chem. Phys.* **1987**, *87*, 115.
(69) Knee, J. L.; Khundkar, L. R.; Zewail, A. H. *J. Chem. Phys.* **1985**, *82*, 4715.
(70) Moss, D. B.; Parmenter, C. S.; Ewing, G. E. *J. Chem. Phys.* **1987**, *86*, 51.
(71) Parmenter, C. S.; Stone, B. M. *J. Chem. Phys.* **1986**, *84*, 4710.
(72) Fischer, G.; Naaman, R. *Chem. Phys.* **1976**, *12*, 367.
(73) Fischer, G.; Knight, A. E. W. *Chem. Phys.* **1976**, *17*, 327.
(74) Wanna, J.; Bernstein, E. R. *J. Chem. Phys.* **1987**, *86*, 6707.
(75) Sur, A.; Johnson, P. M. *J. Chem. Phys.* **1986**, *84*, 1206.
(76) Huang, Z. S.; Jucks, K. W.; Miller, R. E. *J. Chem. Phys.* **1986**, *85*, 6905.
(77) Another nanosecond technique using infrared pump and probe pulses to excite and detect vibrational predissociation of gas-phase hydrogen-bonded clusters is described by Audibert, M.-M.; Palange, E. *Chem. Phys. Lett.* **1983**, *101*, 407.
(78) Smalley, R. E.; Levy, D. H.; Wharton, L. *J. Chem Phys.* **1976**, *64*, 3266.
(79) Drobits, J. C.; Lester, M. I. *J. Chem. Phys.* **1988**, *88*, 120; and references therein.
(80) Skene, J. M.; Waterland, R.; Lester, M. I., to be published.
(81) Drobits, J. C.; Skene, J. M.; Lester, M. I. *J. Chem. Phys.* **1986**, *84*, 2896.
(82) Sivakumar, N.; Evard, D. D.; Cline, J. I.; Janda, K. C. *Chem. Phys. Lett.* **1987**, *137*, 403.
(83) Swartz, B. A.; Brinza, D. E.; Western, C. M.; Janda, K. C. *J. Phys. Chem.* **1984**, *88*, 6272.
(84) Hoffbauer, M. A.; Gentry, W. R.; Giese, C. F. In *Laser Induced Processes in Molecules*; Kompa, K., et al., Eds.; Springer-Verlag: West Berlin, 1978; Vol. 6, p 252.
(85) Gentry, W. R. In *Resonances in Electron-Molecule Scattering, van der Waals Molecules and Reactive Chemical Dynamics*; Truhlar, D. G., Ed.; American Chemical Society: Washington, D.C., 1984; p 289.
(86) Casassa, M. P.; Bomse, D. S.; Janda, K. C. *J. Chem. Phys.* **1981**, *74*, 5044.
(87) Gentry, W. R. In *Structure and Dynamics of Weakly Bound Molecular Complexes*; Weber, A., Ed.; D. Reidel Publishing Co.: Dordrecht, 1987; p 467.
(88) Heijmen, B.; Liedenbaum, C.; Stolte, S.; Reuss, J.; *Z. Phys. D* **1987**, *6*, 199.
(89) Baldwin, K. G. H.; Watts, R. O. *J. Chem. Phys.* **1987**, *87*, 873.
(90) Mitchell, A.; McAuliffe, M. J.; Giese, C. F.; Gentry, W. R. *J. Chem. Phys.* **1985**, *83*, 4271.
(91) King, D. S.; Stephenson, J. C. *J. Chem. Phys.* **1985**, *82*, 5286.
(92) Radhakrishnan, G.; Buelow, S.; Wittig, C. *J. Chem. Phys.* **1986**, *84*, 727.
(93) Scherer, N. F.; Khunkdar, L. R.; Bernstein, R. B.; Zewail, A. H. *J. Chem. Phys.* **1987**, *87*, 1451.
(94) Baiocchi, F. A.; Dixon, T. A.; Joyner, C. H.; Klemperer, W. *J. Chem. Phys.* **1981**, *74*, 6544.
(95) Altman, R. S.; Marshal, M. D.; Klemperer, W. *J. Chem. Phys.* **1982**, *77*, 4344.